Structural and magnetic characteristics of monodispersed Fe and oxide-coated Fe cluster assemblies

D. L. Peng, T. Hihara, K. Sumiyama, and H. Morikawa

Articles you may be interested in

A study of the effect of iron island morphology and interface oxidation on the magnetic hysteresis of Fe-MgO (001) thin film composites
J. Appl. Phys. **112**, 013905 (2012); 10.1063/1.4730630

Magnetic properties of monodisperse iron oxide nanoparticles
J. Appl. Phys. **99**, 08N710 (2006); 10.1063/1.2172891

Template-mediated assembly of FePt L 1 0 clusters under external magnetic field
J. Appl. Phys. **97**, 10J304 (2005); 10.1063/1.1846592

Enhancement of magnetic coercivity and macroscopic quantum tunneling in monodispersed Co/CoO cluster assemblies
Appl. Phys. Lett. **75**, 3856 (1999); 10.1063/1.125479

Dependence of exchange anisotropy and coercivity on the Fe–oxide structure in oxygen-passivated Fe nanoparticles
J. Appl. Phys. **85**, 6118 (1999); 10.1063/1.370280

Structural and magnetic characteristics of monodispersed Fe and oxide-coated Fe cluster assemblies

D. L. Peng,[a)] T. Hihara, K. Sumiyama, and H. Morikawa
Department of Materials Science and Engineering, Nagoya Institute of Technology, Nagoya 466-8555, Japan

We systematically studied structural and magnetic characteristics of size- monodispersed Fe and oxide-coated Fe cluster assemblies with the mean cluster sizes of 7–16 nm. Transmission electron microscopy and scanning electron microscopy (SEM) observations show that the Fe clusters in the assemblies maintain their original size at room temperature. In the SEM images, a random stacking of the Fe clusters and a porous structure with a low cluster packing fraction of about 25% are observed. For the Fe cluster assemblies, magnetic coercivity (H_c) at room temperature increases from 4×10^1 to 4×10^2 Oe by increasing the mean cluster size from 7.3 to 16.3 nm. Using the experimental values of the coercivity at $T \geq 100$ K and the fitting values of blocking temperature T_B from $H_c = H_{c0}[1 - (T/T_B)^{1/2}]$, we estimated the values of magnetic anisotropy constant K of the order of 10^6 erg/cm^3 from $T_B = KV/25k_B$, which is larger by an order of magnitude than the bulk Fe value (5×10^5 erg/cm^3). Such a large effective anisotropy at $T \geq 100$ K is ascribed to the large surface anisotropy effects of the small clusters and the low cluster-packing fraction of the Fe cluster assemblies. For the oxide-coated Fe cluster samples, the coercivity strongly depends on the oxygen gas flow rate during deposition, cluster size, and temperature. In the case of a high oxygen gas flow rate (namely high surface-oxidized clusters), the ferrimagnetic oxide shell crystallites also affect the coercivity at $T > 50$ K: The hysteresis loop shift disappears, leading to a complex change in the coercivity and an enhancement of the effective anisotropy constant. © *2002 American Institute of Physics.* [DOI: 10.1063/1.1501754]

I. INTRODUCTION

Nanoscale magnetism currently provides a wealth of scientific interest and of potential applications.[1,2] When the size of magnetic particles is reduced to a few tens of nanometers, they become single domain and, as a consequence, exhibit a number of unique physical properties such as giant magnetoresistance, large coercivity, superparamagnetism, and quantum tunneling of magnetization. If these physical properties were sustained in smaller magnetic particles, we would expect revolutionary changes in a variety of fundamental research and practical applications.[3–10] Simultaneously, nanometer-scale geometrical and chemical controls are requisite to obtain novel magnetic characteristics.

A number of techniques have been developed to synthesize magnetic nanoparticles, for example, colloidal chemistry method,[3,11] inert gas condensation,[12] laser deposition,[13] mechanical attrition,[14] and electrodeposition.[15] We have recently developed the plasma–gas–condensation (PGC)-type cluster beam deposition apparatus,[16] which is a vapor-phase synthesis of clusters. Since metal vapors are produced by sputtering a target material, a wide variety of elements can serve as source materials.[17] Using this system, we can obtain monodispersed transition metal clusters [Cr (Refs. 16 and 18) and Co (Ref. 19)] with the mean diameters d from a few to a few tens of nanometers and the standard deviation less than 10% of d. We have reported characteristic tunnel-type

conductivity, enhanced magnetoresistance,[20] and quantum tunneling-type magnetic relaxation[21] in the core-shell type Co/CoO monodispersed cluster assemblies prepared by this apparatus.

With the rapid development of magnetic recording media, the memory unit size is going down to smaller than 100 nm. Superparamagnetism is a serious problem because the magnetization direction is eliminated by thermal fluctuation. In particular, the superparamagnetism and the coercivity of single-domain particle systems often depends on the size and size distribution of magnetic particles. In order to optimize the magnetic properties of particle- or cluster-assembled materials, control of particle size distribution is also of immense importance. In this article, we deal with the structure and magnetic characteristics of the size-monodispersed Fe and oxide-coated Fe cluster assemblies. We also study a correlation between the coercivity and the flow rate of oxygen gas (namely surface oxidization degree) and discuss enhanced magnetic anisotropy in these monodispersed Fe and oxide-coated Fe cluster assemblies.

II. EXPERIMENT

The samples were prepared by the PGC-type cluster beam deposition apparatus, whose details were described elsewhere.[16,22] We can control the cluster size by changing the flow rate of Ar gas, R_{Ar}, and the flow rate of He gas, R_{He}. For preparation of oxide-coated Fe cluster assemblies, we introduced oxygen gas through a nozzle set near the

---
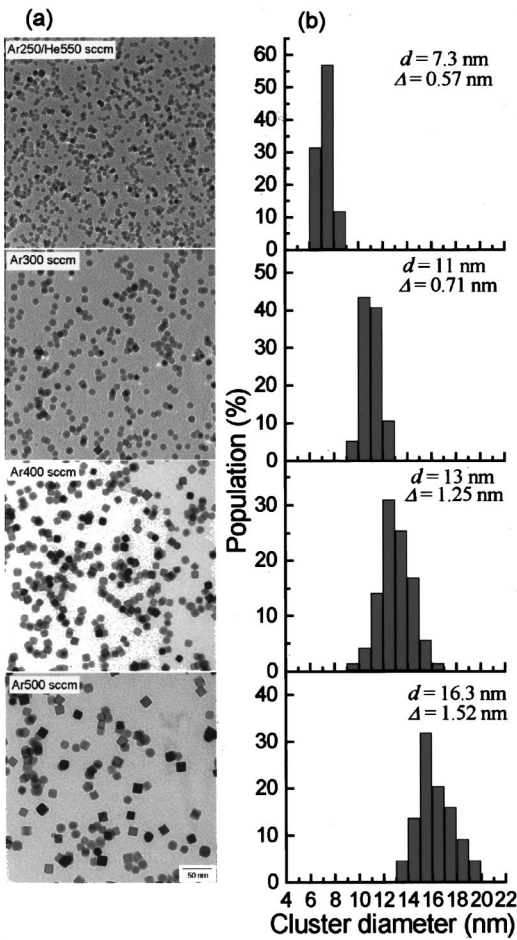[a)]Electronic mail: pengdl@mse.nitech.ac.jp

(a)

FIG. 1. (a) BF-TEM images and (b) size distribution of Fe clusters prepared on a carbon microgrid by varying the Ar gas flow rate R_{Ar} and the He gas flow rate R_{He}.

FIG. 2. ED patterns for Fe clusters with the mean cluster diameter $d=13$ nm prepared on a carbon microgrid at (a) the O_2 gas flow rate $R_{O2}=0$ and (b) 3 sccm, respectively.

skimmer into the deposition chamber to form iron oxide shells covering the Fe clusters before depositing them on the substrate. This process ensures that all Fe clusters are uniformly oxidized before the cluster assemblies are formed. For constant R_{Ar} or $R_{Ar}+R_{He}$, the gas pressure in the deposition chamber can be adjusted lower than 6×10^{-4} Torr by changing the flow rate of oxygen gas (R_{O_2}). We used three kinds of substrates for the Fe cluster deposition: transmission electron microscopy (TEM) microgrids for TEM observations, silicon wafers for scanning electron microscopy (SEM) observations, and polyimide films for magnetic measurement. The effective film thickness of deposited clusters, t_e, was estimated using a quartz crystal thickness monitor, which measures the weight of the deposited clusters. Magnetic measurement was performed using a superconducting quantum interference device magnetometer between 5 and 300 K with the maximum field of 50 kOe.

III. RESULTS

A. Morphology and microstructural characterization

Figure 1(a) shows bright-field (BF)-TEM images of the Fe cluster assemblies with effective thickness $t_e\approx2.5$ nm prepared at $R_{O_2}=0$ sccm. Using an image-analysis software
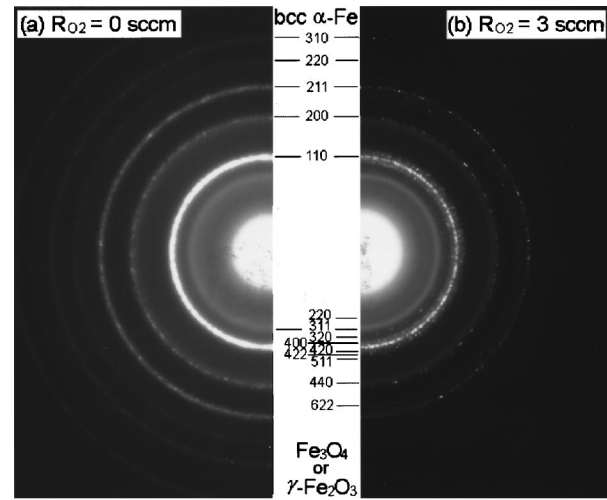
(Image-Pro PLUS: Media Cybernetics), we estimated the size distributions [Fig. 1(b)] of the clusters which do not touch and overlap each other in the digitized images recorded by a slow scan charge coupled device camera in the object area of 350×350 nm^2. As shown here, the mean cluster diameter, d, decreases from 16.3 to 11 nm with decreasing R_{Ar} from 500 to 300 sccm, and further decreases to 7.3 nm with mixing He gas ($R_{He}=550$ sccm) with Ar gas ($R_{Ar}=250$ sccm). The standard deviations (Δ) are less than 10% of d for these samples. These results clearly demonstrate that monodispersed Fe clusters in the size range of about $7-16$ nm are producible by choosing the appropriate R_{Ar} and R_{He} values.

Figures 2(a) and 2(b) show electron diffraction (ED) patterns for the samples with $d=13$ nm prepared at $R_{O_2}=0$ and 3 sccm, respectively. In Fig. 2(a), the diffraction rings indicated by the lines can be mainly indexed as {110}, {200}, {211}, {220}, and {310} of body-centered-cubic (bcc) α-Fe phase. There is a ring corresponding to {311} of Fe$_3$O$_4$ or γ-Fe$_2$O$_3$ phase, where it is not possible to differentiate between these two phases by ED because their lattice parameters are very similar. This is due to partial oxidation of the cluster assembly only by exposing it to the ambient atmosphere. In Fig. 2(b), it is evident that α-Fe phase and Fe$_3$O$_4$ or γ-Fe$_2$O$_3$ phase coexist. The intensity and number of the oxide phase rings for the sample produced at $R_{O_2}=3$ sccm [Fig. 2(b)] is much stronger than those at $R_{O_2}=0$ sccm [Fig. 2(a)].

Figure 3(a) shows BF-TEM micrograph of the oxide-coated Fe cluster assemblies with $d=13$ nm and the effective thickness $t_e\approx2.5$ nm prepared at $R_{O_2}=3$ sccm. Almost all clusters are characterized with a strong contrast in their "core", but with a uniform gray contrast in their "shell". Figure 3(b) shows a high-resolution TEM micrograph of the core-shell cluster observed in the same aggregate. The lattice fringe 0.203 nm shown by two arrows in the core is attributable to the α-Fe phase while the lattice fringes 0.253 nm shown by three arrows in the shell to the {311} spacing of
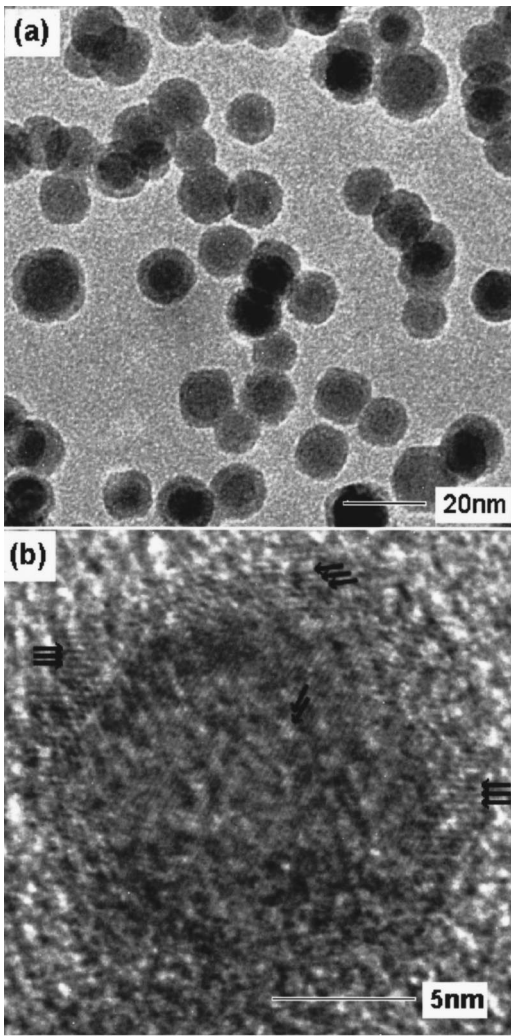
FIG. 3. (a)BF-TEM micrograph of the oxide-coatedFe clusters with $d = 13$ nm prepared on a carbon microgrid at the O_2 gas flow rate $R_{O_2} = 3$ sccm. Almost all clusters show a core-shell structure. (b) High-resolution TEM micrograph of an oxide-coated Fe cluster, found in the same cluster sample. The lattice fringe indicated by two arrows in the core region corresponds to the {110} lattice spacing (0.203 nm) of the bcc α-Fe phase, while those indicated by three arrows in the shell region are for the {311} lattice spacing (0.253 nm) of the Fe_3O_4 or γ-Fe_2O_3 phase.

Fe_3O_4 or γ-Fe_2O_3 phase. These results also indicate that the oxide-coated Fe clusters were covered with the Fe_3O_4 or γ-Fe_2O_3 shells composed of very small crystallites.

We also observed the morphology of Fe cluster-assembled films with a high-resolution SEM (HITACHI: S-4700) operating at 15 kV. Figures 4(a) and 4(b) show the plan-view and cross-sectional SEM images of the size-monodispersed Fe cluster assembly with $d = 13$ nm. The plan-view image reveals very bumpy film surfaces containing inhomogeneous aggregation of Fe clusters. In the cross-sectional image, we observe a random stacking of the Fe clusters. In those images, individual Fe clusters are distinguishable. This suggests that the Fe clusters in the assemblies maintain their original size at room temperature. The actual thickness estimated from low-magnification cross-sectional SEM image is about $t_a = 800$ nm, while the effective thickness estimated from the thickness monitor was $t_e = 200$ nm,
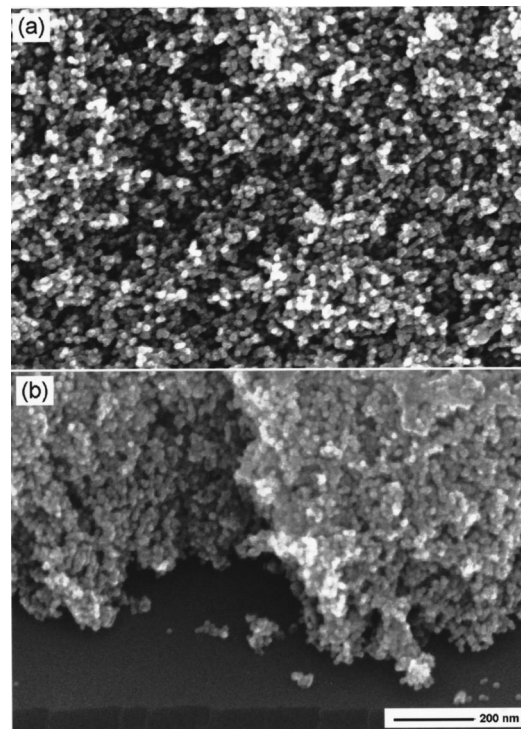

FIG. 4. (a) Plan-view and (b) cross-sectional SEM image of the Fe cluster assemblies with $d = 13$ nm.

i.e., t_a is about four times of t_e. This implies that the cluster-assembled films are very porous and have a cluster packing fraction of about 25% ($= t_e/t_a = 200$ nm/800 nm).

B. Magnetic behaviors of Fe cluster assemblies

Figure 5 shows the temperature (T) dependence of coercivity H_c for the Fe cluster assemblies prepared at $R_{O2} = 0$ sccm:$d = 7.3$, 9, 13, and 16.3 nm. Their effective thickness is $t_e \approx 200$ nm. For the large size clusters ($d = 13$ and 16.3 nm), H_c increases gradually with decreasing T; while for small size clusters ($d = 7.3$ and 9 nm), H_c rapidly increases with decreasing T at low temperatures ($T < 100$ K). For $d = 7.3$ nm, for instance, H_c increases from 4×10^1 to 8.3×10^2 Oe when T is decreased from 300 to 5 K. The large H_c values at
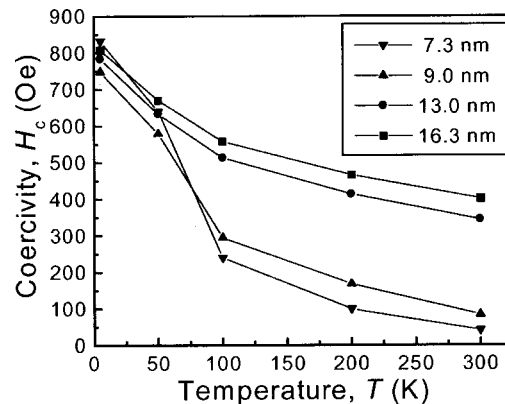

FIG. 5. Temperature dependence of coercivity H_c for the Fe cluster assemblies with the thickness $t_e = 200$ nm and the mean cluster diameter $d = 7.3$, 9, 13, and 16.3 nm.
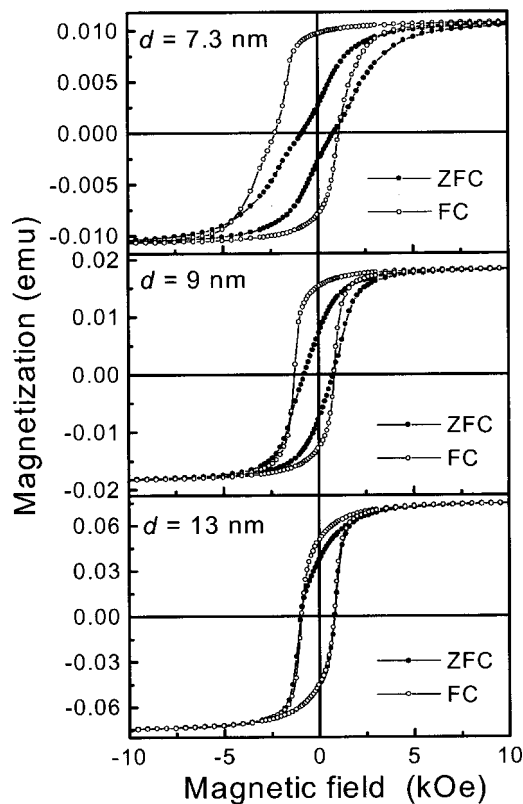
FIG. 6. Hysteresis loops of the ZFC and FC monodispersed Fe cluster assemblies with $d=7.3$, 9, and 13 nm.

FIG. 7. Hysteresis loops of the ZFC and FC oxide-coated Fe cluster assemblies with $d=9$ nm prepared at $R_{O_2}=0$, 1, and 3 sccm.

low temperatures are ascribed to both an intrinsic property of ferromagnetic single-domain Fe particles and an extrinsic property of the exchange anisotropy.[23] Note that the latter originates from the presence of an antiferromagnetic oxide layers covering the ferromagnetic clusters,[24,25] although the oxide layers were identified to be two ferrimagnetic phases.

To confirm the presence of the exchange anisotropy, we measured the hysteresis loops at 5 K after zero-field cooling (ZFC) and field cooling (FC) the samples from 300 to 5 K in a magnetic field, H, of 20 kOe. The direction of H used to measure the loops was parallel to that of the cooling field. Figure 6 shows the ZFC and FC loops of the monodispersed Fe cluster assemblies with $d=7.3$, 9 and 13 nm prepared at $R_{O_2}=0$ sccm. For two samples with $d=7.3$ and 9 nm, the large shift of the FC loop in comparison with the symmetric feature in the ZFC loop is detected, which confirms the presence of the unidirectional exchange anisotropy.[25] This is due to partial surface oxidation of the cluster assembly only by exposing it to the ambient atmosphere. For the sample with $d=13$ nm, the loop shift is not so marked but the loop shape is changed slightly. In addition, comparing the ZFC loops for these Fe cluster assemblies, we can see that the magnetization is saturated more easily with increasing d. These features are ascribed to the exchange anisotropy effect depending on the volume fraction of the Fe core and the oxide shell.

C. Magnetic behaviors of oxide-coated Fe cluster assemblies
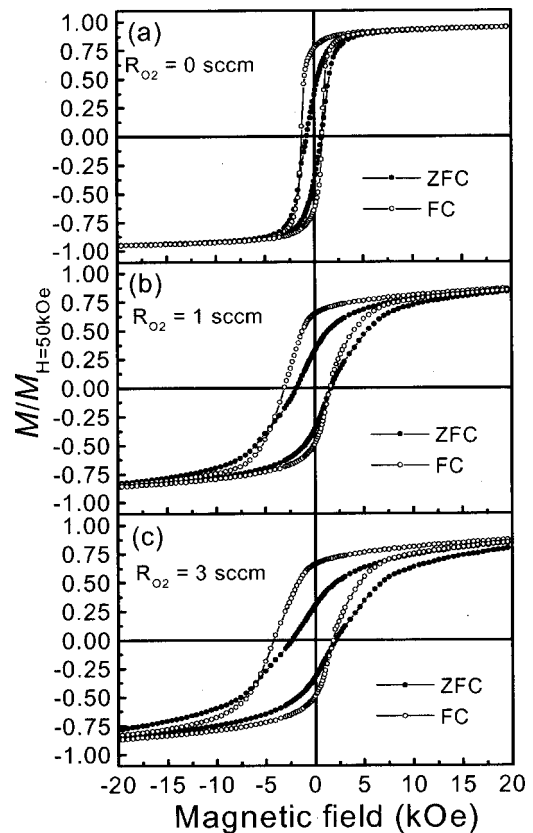
Figure 7 shows the ZFC and FC loops of the oxide-

coated Fe cluster assemblies with $d=9$ nm prepared at $R_{O_2}=0$, 1 and 3 sccm. H_c (in both ZFC and FC cases) and the loop shift increases with increasing R_{O_2}. At room temperature, however, H_c becomes smaller with introducing O_2 gas (Fig. 8). These results indicate that the volume or thickness of the oxide shells increases and the volume of Fe cores decreases with increasing R_{O_2}. In addition, as is seen from Figs. 7 and 8, the magnetization is saturated more slowly with increasing R_{O_2} at both 5 K and room temperature. In particular, at room temperature, relative magnetization $M/M_{H=1500\ Oe}$ of the oxide-coated Fe cluster assembly
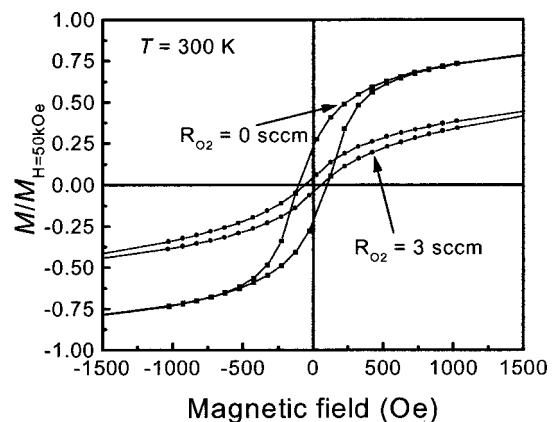

FIG. 8. Hysteresis loops at room temperature for the oxide-coated Fe cluster assemblies with $d=9$ nm prepared at $R_{O_2}=0$ and 3 sccm.
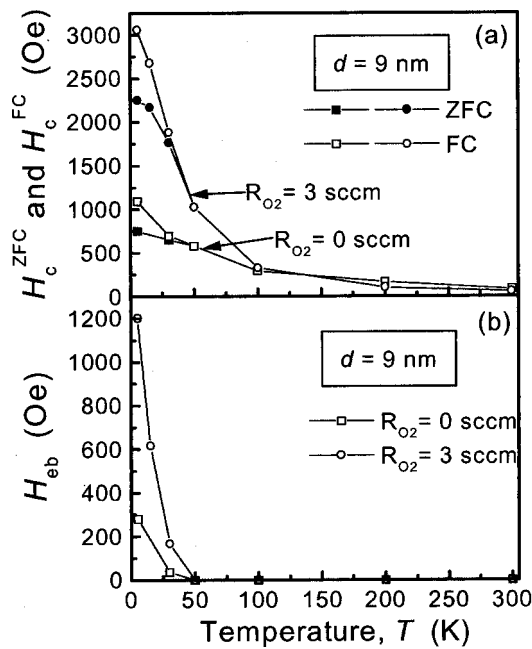
FIG. 9. (a) Coercivities, H_c^{FC} and H_c^{FC}, of the ZFC and FC samples and (b) exchange bias field H_{eb} as a function of temperature, T, for the oxide-coated Fe cluster assemblies with $d=9$ nm prepared at $R_{O_2}=0$ and 3 sccm.

FIG. 10. ZFC and FC magnetization as a function of temperature from 300 to 5 K for the oxide-coated Fe cluster assemblies with $d=9$ nm prepared at (a) $R_{O_2}=0$ and (b) 1 sccm. The measuring field and the cooling field, H, are 100 Oe.

$(R_{O_2}=3$ sccm) is decreased to about half of that of the Fe cluster assembly $(R_{O_2}=0$ sccm). These features are ascribed to the exchange interaction at low temperature mentioned herein as well as superparamagnetism of the oxide shell crystallites at room temperature.

Figures 9(a) and 9(b) show coercivities, H_c^{ZFC} and H_c^{FC}, of the ZFC and FC sample and exchange bias field H_{eb} as a function of temperature for the cluster assemblies with $d=9$ nm prepared at $R_{O_2}=0$ and 3 sccm. For the FC sample, H_c^{FC} is defined as the average of the positive and negative field values. The difference in H_c^{ZFC} and H_c^{FC} becomes more significant with decreasing T for both $R_{O_2}=0$ and 3 sccm. Such a bifurcation effect starts at about $T=50$ K. H_{eb} also rapidly decreases with increasing T and becomes negligibly small above $T=50$ K. This indicates that unidirectional exchange anisotropy (UEA) disappears at about $T=50$ K.

Figure 10 shows the ZFC and FC magnetization as a function of temperature from 300 to 5 K for the cluster assemblies with $d=9$ nm prepared at $R_{O_2}=0$ and 1 sccm. For the ZFC measurement, the sample was cooled in the absence of an external magnetic field from $T=300$ to 5 K. Then H $(=100$ Oe) was applied and the magnetization was measured with increasing temperature. For the FC measurement, the sample was cooled in the presence of $H=100$ Oe from T $=300$ to 5 K, and then the magnetization was measured with increasing temperature at $H=100$ Oe. As seen from Fig. 10, a distinct magnetic cooling effect is observed for both samples. From 50 to 300 K, the ZFC magnetization monotonically increases for $R_{O_2}=0$ sccm and the FC magnetization does not change over this temperature range, showing a ferromagnetic behavior. For $R_{O_2}=1$ sccm, the ZFC magnetization rapidly increases from 50 to 150 K and then slightly increases with increasing T; the FC magnetization reveals a
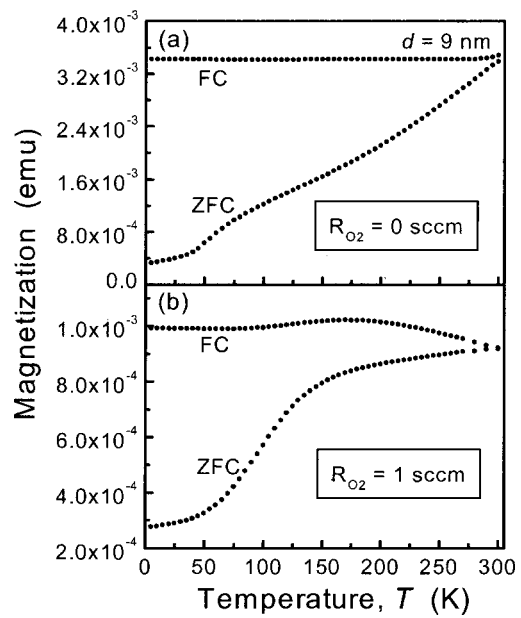
broad peak at about 175 K, which may be related to a superparamagnetic behavior of the oxide shell crystallites whose sizes are widely distributed.

Figure 11 shows the ZFC and FC magnetization as a function of temperature from 300 to 5 K at applied fields $H=100$, 20 000, and 50 000 Oe for the cluster assemblies with $d=9$ nm prepared at $R_{O_2}=3$ sccm. The low-field $(H$ $=100$ Oe) thermomagnetic curves [Fig. 11(a)] show the same features as these for $R_{O_2}=1$ sccm [Fig. 10(b)]. For the high-field $(H=20\,000$ and 50 000 Oe) thermomagnetic curves [Figs. 11(b) and 11(c)], the ZFC magnetization increases up to approximately $T_{max}=40$–60 K and then decreases smoothly up to room temperature. On the other hand, it is also evident from Figs. 11(b) and 11(c) that the ZFC and FC magnetizations do not coincide completely each other even at much higher temperatures than T_{max}. These features indicate that there is a strong interaction between the Fe cores or between the Fe cores and the oxide shells.

D. Training effect

In order to further investigate the exchange anisotropy, we measured the dependence of the exchange bias field H_{eb} on repeated magnetization reversals, namely the so-called training effect which is a diminution of H_{eb} upon the subsequent magnetization reversals.[10] Figure 12(a) shows typical results from the loops measured along the field-cooling direction at 5 K for the oxide-coated Fe cluster assembly with $d=9$ nm and $R_{O_2}=3$ sccm. The successive loops do not coincide with each other and show a decrease in H_{eb}. Figure 12(b) shows the dependence of H_{eb} and the training effect on the training cycle number at 5 K. Here, we define the training effect as the fraction of the initial value which is lost after field cycling. The decrease of H_{eb} is remarkable by increas-
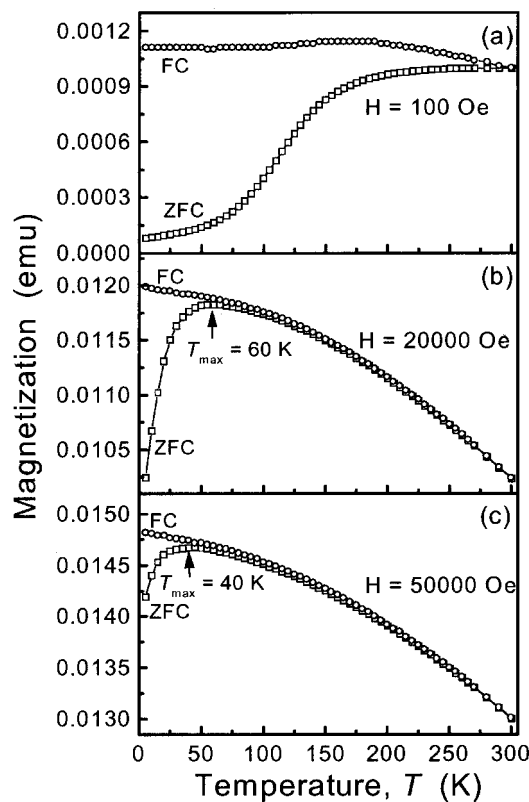
FIG. 11. ZFC and FC magnetization as a function of temperature from 300 to 5 K for the oxide-coated Fe cluster assemblies with $d = 9$ nm prepared at $R_{O_2} = 3$ sccm. The measuring field and the cooling field are as follows: (a) $H = 100$, (b) 20 000, and (c) 50 000 Oe.

FIG. 12. (a) Successive hystersis loops measured at 5 K after cooling from 300 K in a field of $+20\,000$ Oe along the same direction; (b) H_{eb} and training effect as a function of the training cycle number for the oxide-coated Fe cluster assembly with $d = 9$ nm prepared at $R_{O_2} = 3$ sccm.

ing the training cycle number and the training effect is decreased to about 30% after the 13th cycle. This result is clearly different from that of the monodispersed CoO-coated Co cluster assembly, in which the decrease of H_{eb} is larger for the second cycle, and then become almost constant after further numbers of the training cycles; the training effect is only deceased to about 89% after the 14th cycle.[21] This suggests that the training effect strongly depends on magnetic properties of the oxide shells, namely antiferromagnetism or ferrimagnetism.

IV. DISCUSSION

As described in Secs. III B and III C, UEA are observed at low temperatures. The bifurcation effect between H_c^{ZFC} and H_c^{FC} and the shift of the FC hysteresis loop become negligibly small above $T = 50$ K, which is much lower than the magnetic transition temperature of the bulk Fe_3O_4 ($T_c = 858$ K) or γ-Fe_2O_3 ($T_c = 860$ K). Similar results for oxide-coated Fe fine particles were already observed by Gangopadhyay *et al.*[26] and attributed to the superparamagnetic behavior of the ferrimagnetic oxide shell with very small crystallites above a blocking temperature (30–40 K). However, for the oxide-coated Fe clusters, spin orientation at and near the core-shell interface should be different from that for simple ferromagnetic/ferrimagnetic bilayers because of the small size of cores and shell crystallites. For example, a Mössbauer spectroscopy study on surface oxidized Fe nanoparticles revealed that the surface shell consisted of very
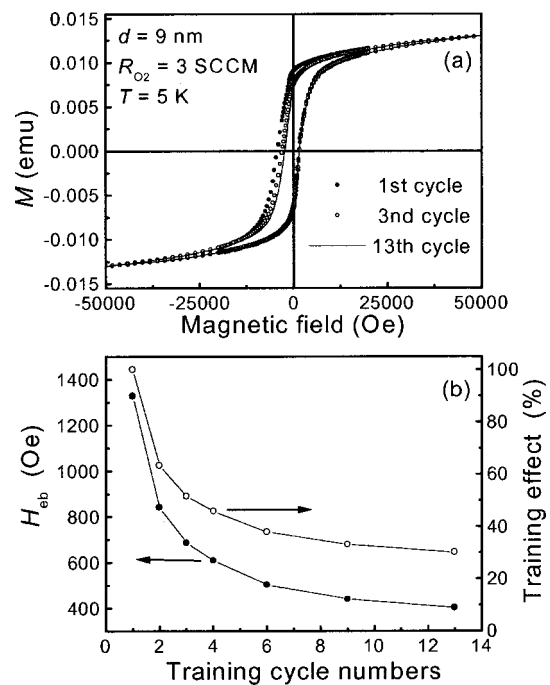
small crystallites and that a large spin canting characterized the oxide phase.[27–29] In ferrite nanoparticles, a surface spin disorder has been experimentally discussed,[30–32] being corroborated by numerical calculations. The antiferromagnetic superexchange interaction is disrupted at the surface of the ferrimagnetic oxide crystallites because of missing oxygen ions or presence of other impurity molecules. Such broken exchange bonds between surface spins lead to surface spin disorder, being compatible with a spin-glasslike behavior at the surface. Therefore, the hypothesis of spin disorder at the surface of the oxide crystallites or the interface of the Fe core and oxide shell is applicable for the present oxide-coated Fe cluster assemblies. According to this hypothesis, the onset of loop shift and bifurcation between H_c^{ZFC} and H_c^{FC} below about $T = 50$ K can be ascribed to a freezing of disorder surface spins of the oxide shell crystallites. The presence of such a disordered spin freezing state leads to not only the loop shift but also the large H_c which is much larger than the intrinsic value of the Fe core, because an ideal interface between the Fe core and oxide shell should have no effect on the enhancement of H_c. Our measurement result of the training effect (Fig. 12) also further supports such a hypothesis of the spin-glasslike state in the interfacial layers between the Fe core and oxide shell. The repeated magnetization reserval at high fields makes the interfacial spins change to a new frozen spin state and decreases the net interfacial uncompensated antiferromagnetlike magnetization, causing a decrease of H_{eb} and H_c.

We also observed in Sec. III that H_c is also strongly influenced by the cluster size, temperature, and surface oxidization degree of the clusters. For the present monodispersed Fe and oxide-coated cluster assemblies, the cluster

TABLE I. Coercivity values observed and values of the effective magnetic anisotropy constant K_{eff} obtained by H_c versus $T^{1/2}$ law.

	H_c (Oe)		K_{eff} (erg/cm^3)
d (nm)	($T = 300$ K)	($T = 5$ K)	($T \geq 100$ K)
7.3	41	833	...
9.0	84	748	3.66×10^6
13.0	343	784	3.09×10^6
16.3	401	807	1.97×10^6

FIG. 13. Coercivity H_c at $T \geq 100$ K as a function of $T^{1/2}$ for the monodispersed Fe cluster assemblies with $d = 7.3$, 9, 13, and 16.3 nm prepared at $R_{O_2} = 0$ sccm. Solid lines show the H_c versus $T^{1/2}$ fitting. Except for $d = 7.3$ nm, the fitting is pretty satisfactory.

size dependence of H_c below about $T = 50$ K becomes complex because of exchange anisotropy effect, which is decided by the volume fraction of the Fe core and the oxide shell. Therefore, we only discuss the H_c value and magnetic anisotropy at $T \geq 100$ K as follows. For all samples obtained in the present work, each Fe cluster should have a single-domain structure since their sizes are smaller than the critical particle diameter (about 23 nm) below which the formation of domain walls becomes unfavorable.[33] According to the simple theory on a random assembly of single-domain particles, the magnetic coercivity is expressed as[34,35]

$$H_c^{max} = p_c K_1 / M_s, \tag{1}$$

where K_1 is the magnetocrystalline anisotropy constant, M_s is saturation magnetization, and p_c is a constant defined by the crystalline symmetry, orientation, and grain shape: For instance, p_c is 0.64 for ensembles of randomly oriented cubic-crystal particles. Thus, H_c^{max} is independent of d in this relation. For an α-Fe particle system, we estimate from Eq. (1) that the H_c^I value is about 190 Oe using the reported values of $K_1 = 5 \times 10^5$ erg/cm^3 and $M_s = 219$ emu/g for the bulk Fe.[36] Moreover, since H_c depends on a packing density of magnetic particles, the observed H_c is empirically related to the ideal H_c^I as follows: $H_c = (1 - P) H_c^{max}$, where P is the packing fraction of the clusters.[37] The P value estimated from Fig. 4 is about $P = 25\%$, resulting in $H_c = 140$ Oe. At $T = 300$ K, this value is comparable to the H_c values (see Table I) observed for the present Fe cluster assemblies with the porous structure while it is much larger than those of the samples with $d = 7.3$ and 9 nm, and smaller than those of the samples with $d = 13$ and 16.3 nm.

We also tried to further clarify magnetic characteristics of the Fe cluster assemblies. Attempts were made to calculate the value of the effective anisotropy constant K_{eff} from the temperature dependence of the coercivity at $T \geq 100$ K in which the exchange anisotropy effect between the Fe core and oxide shell disappears. For single-domain ferromagnetic particles having no interaction between them, the coercivity is given by[38]

$$H_c = 2 K_{eff} / M_s [1 - (25 k_B T / K_{eff} V)^{1/2}] = H_{c,0}[1 - (T/T_B)^{1/2}], \tag{2}$$

where V is the volume of the ferromagnetic particle and k_B is the Boltzmann constant. $H_{c,0} = 2 K_{eff} / M_s$ is the coercivity at $T = 0$ K. Equation (2) predicts that the value of H_c increases as the cluster size becomes larger. This is consistent with the observed results shown in Table I. Moreover, as shown in
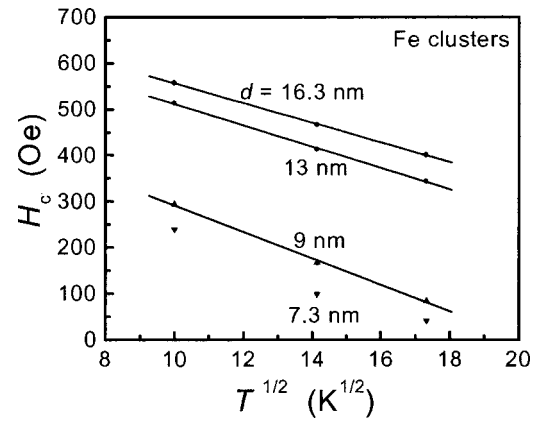
Fig. 13, except for $d = 7.3$ nm, the Fe clusters closely follow this relationship [Eq. (2)] and the fitting is satisfactory. The values of K_{eff} from this fit are listed in Table I. The H_c versus $T^{1/2}$ law gave values of K_{eff} of the order of 10^6 erg/cm^3. Thus the experimental value (K_{eff}) of the anisotropy constant is larger by an order of magnitude than the bulk Fe and Fe-oxide values. In addition, as seen from Table I, K_{eff} increases with decreasing the cluster size.

Moreover, we analyzed the anisotropy for the oxide-coated Fe clusters. Figures 14(a) and 14(b) show that the variation of H_c with temperature for the oxide-coated Fe cluster assemblies with $d = 13$ and 9 nm. In both cases, H_c is
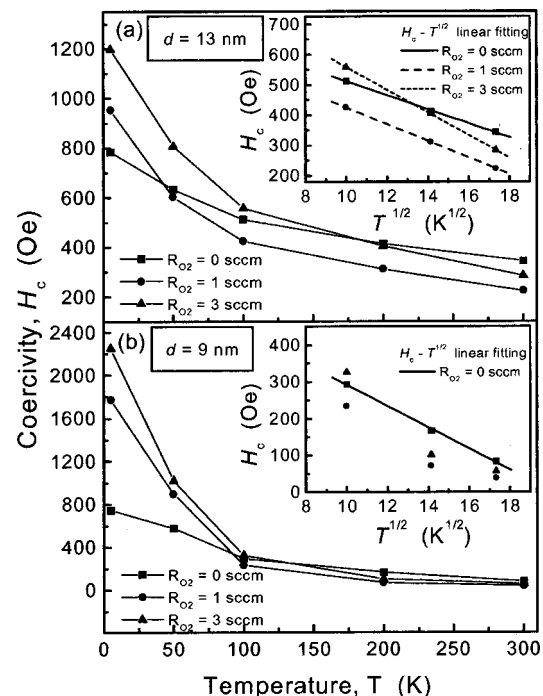

FIG. 14. Variation of coercivity, H_c, with temperature for the oxide-coated Fe cluster assemblies (a) with $d = 13$, and (b) 9 nm prepared at $R_{O_2} = 0$, 1, and 3 sccm. The insets show the results of the H_c versus $T^{1/2}$ fitting at the temperature range of $T \geq 100$ K.

dependent on R_{O_2}. When $R_{O_2}=1$ sccm, H_c is smaller than that for $R_{O_2}=0$ sccm at $T \geqslant 100$ K. However, when $R_{O_2}=3$ sccm, H_c is larger than that for $R_{O_2}=1$ sccm at all temperature ranges and is smaller than that for $R_{O_2}=0$ sccm only at $T>100$ K. The inset of Fig. 14(a) clearly shows that for $d=13$ nm, the H_c versus $T^{1/2}$ fitting is pretty satisfactory not only at $R_{O_2}=0$ sccm but also at $R_{O_2}=1$ and 3 sccm, while the inset of Fig. 14(b) shows that for $d=9$ nm, the H_c versus $T^{1/2}$ law is unsuitable with increasing R_{O_2}, similar to the case of the Fe cluster assembly with $d=7.3$ nm (Fig. 13). These behaviors evidently result from the volume fraction of the Fe core and oxide shell: for same size clusters the diameter of Fe cores is decreased and the thickness of the oxide shells is increased with increasing R_{O_2}. These results suggest that, even at $T \geqslant 100$ K, when R_{O_2} becomes larger than a certain value, the ferrimagnetic oxide shell crystallites dominate the coercivity of cluster assembly by strong interaction between the Fe cores and the oxide shell crystallites as well as intrinsic anisotropy of the oxide shell crystallites. Moreover, with decreasing size of the Fe cores, the surface anisotropy effect[39–41] also becomes more remarkable. All of these factors lead to enhancement of magnetic anisotropy. Indeed, from the inset of Fig. 14(a), the H_c versus $T^{1/2}$ fitting gives the K_{eff} values of 3.09×10^6, 4.29×10^6, and 5.63×10^6 erg/cm^3 for $R_{O_2}=0$, 1, and 3 sccm, respectively. Here, we used the Fe core diameters: 10 and 9 nm, and the thickness of the oxide shell: 1.5 and 2 nm for $R_{O_2}=1$ and 3 sccm, respectively, according to our high-resolution TEM observation. The fitting result shows that K_{eff} increases with R_{O_2}. In addition, based on the aforementioned consideration, we can also explain why the values of H_c for $d=9$ nm do not satisfy the H_c versus $T^{1/2}$ law when $R_{O_2}=1$ and 3 sccm. This can be ascribed to the competitive anisotropies of the Fe cores and the oxide shell crystallites. In other words, the anisotropy of the Fe cores has not been clear predominantly in the oxide-coated Fe cluster assemblies with the small cluster size.

V. CONCLUSIONS

Using the PGC-type cluster beam deposition technique, we have produced the monodispersed Fe cluster assemblies with a mean diameter of $d=7.3$–16.3 nm. By surface oxidation process under low O_2 pressure ($<6 \times 10^{-4}$ Torr), the monodispersed Fe cluster assemblies covered by the Fe_3O_4 or γ-Fe_2O_3 shells are also obtained. Random stacking of Fe clusters leads to a very porous assembly structure and individual Fe clusters are distinguishable, suggesting that the Fe clusters in the assemblies maintain their original size at room temperature. For the oxide-coated Fe cluster assemblies, H_c and H_{eb} strongly depend on the cluster size, temperature, and surface oxidization degree of the clusters. The decrease of H_{eb} is remarkable by increasing the training cycle number and the training effect is decreased to about 30% after the 13th cycle, being different from that of the monodispersed CoO-coated Co cluster assembly. The onset of loop shift and bifurcation between H_c^{ZFC} and H_c^{FC} below about $T=50$ K can be ascribed to an exchange interaction between the ferromag-

netic Fe core and the freezing layers of disordered surface spins of the oxide shell crystallites, which is also the predominant origin to an enhancement of the magnetic anisotropy at low temperature. At the temperature range from 100 to 300 K, however, the large H_c and enhanced magnetic anisotropy in the cluster assemblies are believed to result from the surface anisotropy effect of the small ferromagnetic clusters and the low cluster-packing fraction of the Fe cluster assemblies.

[1] D. L. Leslie-Pelecky and R. D. Rieke, Chem. Mater. **8**, 1770 (1996).
[2] *Nanomaterials: Synthesis, Properties and Applications*, edited by A. S. Edelstein and R. C. Cammarata (Institute of Physics, Bristol, 1996).
[3] C. T. Black, C. B. Murray, R. L. Sandstrom, and S. Sun, Science **290**, 1131 (2000).
[4] J. A. Katine, F. J. Albert, and R. A. Buhrman, Appl. Phys. Lett. **76**, 354 (2000).
[5] E. Girt, Kannan M. Krishnan, G. Thomas, and Z. Altounian, Appl. Phys. Lett. **76**, 1746 (2000).
[6] B. Bian, D. E. Laughlin, K. Sato, and Y. Hirotsu, J. Appl. Phys. **87**, 6962 (2000).
[7] D. L. Peng, K. Sumiyama, T. Hihara, and S. Yamamuro, Appl. Phys. Lett. **75**, 3856 (1999).
[8] Y. Peng, H.-L. Zhang, S.-L. Pan, and H.-L. Li, J. Appl. Phys. **87**, 7405 (2000).
[9] S. P. Li, W. S. Lew, Y. B. Xu, A. Hirohata, A. Samad, F. Baker, and J. A. C. Bland, Appl. Phys. Lett. **76**, 748 (2000).
[10] M. Holdenried, B. Hackenbroich, and M. Micklitz, J. Magn. Magn. Mater. **231**, L13 (2001).
[11] S. Sun and C. B. Murray, J. Appl. Phys. **85**, 4325 (1999).
[12] H. Gleiter, Prog. Mater. Sci. **33**, 223 (1989).
[13] S. S. Parkin, N. More, and K. P. Roche, Phys. Rev. Lett. **64**, 2304 (1990).
[14] C. C. Koch, Nanostruct. Mater. **9**, 13 (1997).
[15] S. Banerjee, S. Roy, J. W. Chen, and D. Chakravorty, J. Magn. Magn. Mater. **219**, 45 (2000).
[16] S. Yamamuro, K. Sumiyama, M. Sakurai, and K. Suzuki, Supramol. Sci. **5**, 239 (1998).
[17] H. Haberland, M. Karrais, M. Mall, and Y. Thurner, J. Vac. Sci. Technol. A **10**, 3266 (1992).
[18] S. Yamauro, K. Sumiyama, and K. Suzuki, J. Appl. Phys. **85**, 483 (1999).
[19] S. Yamamuro, K. Sumiyama, T. J. Konno, and K. Suzuki, Mater. Trans., JIM **40**, 1450 (1999).
[20] D. L. Peng, K. Sumiyama, T. J. Konno, T. Hihara, and S. Yamamuro, Phys. Rev. B **60**, 2093 (1999).
[21] D. L. Peng, K. Sumiyama, T. Hihara, S. Yamamuro, and T. J. Konno, Phys. Rev. B **61**, 3103 (2000).
[22] D. L. Peng, K. Sumiyama, T. Hihara, and T. J. Konno, Scr. Mater. **44**, 1471 (2001).
[23] S. Gangopadhyay, G. C. Hadjipanayis, B. Dale, C. M. Sorensen, K. J. Klabunde, V. Papaefthymiou, and A. Kostikas, Phys. Rev. B **45**, 9778 (1992).
[24] B. D. Cullity, in *Introduction to Magnetic Materials* (Addison–Wesley, London, 1972), p. 423.
[25] W. H. Meiklejohn and C. P. Bean, Phys. Rev. **102**, 1413 (1956); *ibid.* **105**, 904 (1957).
[26] S. Gangopadhyay, G. C. Hadjipanayis, B. Dale, C. M. Sorensen, and K. J. Klabunde, Nanostruct. Mater. **1**, 77 (1992).
[27] K. Haneda and A. H. Morrish, Surf. Sci. **77**, 584 (1978).
[28] S. Linderoth, S. Morup, and M. D. Bentzon, J. Mater. Sci. **30**, 3142 (1995).

[29] L. Bel Bianco, A. Hernando, E. Bonetti, and E. Navarro, Phys. Rev. B **56**, 8894 (1997).
[30] R. H. Kodama, A. E. Berkowitz, E. J. McNiff, and S. Foner, Phys. Rev. Lett. **77**, 394 (1996).
[31] R. H. Kodama and A. S. Edelstein, J. Appl. Phys. **85**, 4316 (1999).
[32] L. Del Bianco, A. Hernando, M. Multigner, C. Prados, J. C. Sanchez-Lopez, A. Fernandez, C. F. Conde, and A. Conde, J. Appl. Phys. **84**, 2189 (1998).
[33] O. Kitakami, T. Sakurai, Y. Miyashita, Y. Takeno, and Y. Shimada, Jpn. J. Appl. Phys., Part 1 **35**, 1724 (1996).
[34] A. H. Morrish, *The Physical Principles of Magnetism* (Wiley, New York, 1965), p. 354.
[35] E. C. Stoner and E. P. Wohlfarth, Proc. Phys. Soc. Jpn. **240**, 599 (1948).
[36] F. Sato, N. Tezuka, T. Sakurai, and T. Miyazaki, J. Magn. Soc. Jpn. **17**, 886 (1993).
[37] R. M. Bozorth, *Ferromagnetism* (IEEE, New York, 1978), p. 831.
[38] E. H. Frei, S. Shtrikman, and D. Treves, Phys. Rev. **106**, 446 (1957).
[39] M. Respaud, J. M. Broto, H. Rakoto, A. R. Fert, L. Thomas, B. Barbara, M. Verelst, E. Snoeck, P. Lecante, A. Mosset, J. Osuna, T. O. Ely, C. Amiens, and B. Chaudret, Phys. Rev. B **57**, 2925 (1998).
[40] C. Chen, O. Kitakami, and Y. Shimada, J. Appl. Phys. **84**, 2184 (1998).
[41] F. Bodker, S. Mϕrup, and S. Linderoth, Phys. Rev. Lett. **72**, 282 (1994).